Therapeutic impacts of GNE-477-loaded H_2O_2 stimulus-responsive dodecanoic acid-phenylborate ester-dextran polymeric micelles on osteosarcoma

SONGMU PAN[1*], ZHUAN ZOU[1*], XIAOFENG ZHOU[1], JIYONG WEI[1], HUIJIANG LIU[1], ZHONGYI SU[1], GUI LIAO[1], GUANGYU HUANG[1], ZONGGUI HUANG[1], YI XU[2], MINAN LU[3] and RONGHE GU[1,4]

[1]Department of Orthopedic Surgery, The First People's Hospital of Nanning, The Fifth Affiliated Hospital of Guangxi Medical University, Nanning, Guangxi 530022, P.R. China; [2]Department of Pharmacy, First Affiliated Hospital of Wenzhou Medical University, Wenzhou, Zhejiang 325000, P.R. China; [3]Department of Orthopedic Surgery, The Affiliated Hospital of Youjiang Medical University for Nationalities, Baise, Guangxi 533000, P.R. China; [4]Guangxi Key Laboratory of Intelligent Precision Medicine, The First People's Hospital of Nanning, The Fifth Affiliated Hospital of Guangxi Medical University, Nanning, Guangxi 530022, P.R. China

Received December 19, 2023; Accepted April 25, 2024

DOI: 10.3892/ijmm.2024.5393

Abstract. Osteosarcoma (OS) is a highly malignant primary bone neoplasm that is the leading cause of cancer-associated death in young people. GNE-477 belongs to the second generation of mTOR inhibitors and possesses promising potential in the treatment of OS but dose tolerance and drug toxicity limit its development and utilization. The present study aimed to prepare a novel H_2O_2 stimulus-responsive dodecanoic acid (DA)-phenylborate ester-dextran (DA-B-DEX) polymeric micelle delivery system for GNE-477 and evaluate its efficacy. The polymer micelles were characterized by morphology, size and critical micelle concentration. The GNE-477 loaded DA-B-DEX (GNE-477@DBD) tumor-targeting drug delivery system was established and the release of GNE-477 was measured. The cellular uptake of GNE-477@DBD by three OS cell lines (MG-63, U2OS and 143B cells) was analyzed utilizing a fluorescent tracer technique. The hydroxylated DA-B was successfully grafted onto dextran at a grafting rate of 3%, suitable for forming amphiphilic micelles. Following exposure to H_2O_2, the DA-B-DEX micelles ruptured and released the drug rapidly, leading to increased uptake of GNE-477@DBD by cells with sustained release of GNE-477. The *in vitro* experiments, including MTT assay, flow cytometry, western blotting and RT-qPCR, demonstrated that GNE-477@DBD inhibited tumor cell viability, arrested cell cycle in G1 phase, induced apoptosis and blocked the PI3K/Akt/mTOR cascade response. *In vivo*, through the observation of mice tumor growth and the results of H&E staining, the GNE-477@DBD group exhibited more positive therapeutic outcomes than the free drug group with almost no adverse effects on other organs. In conclusion, H_2O_2-responsive DA-B-DEX presents a promising delivery system for hydrophobic anti-tumor drugs for OS therapy.

Correspondence to: Dr Ronghe Gu, Department of Orthopedic Surgery, The First People's Hospital of Nanning, The Fifth Affiliated Hospital of Guangxi Medical University, 89 Qixing Road, Nanning, Guangxi 530022, P.R. China
E-mail: 201920518@sr.gxmu.edu.cn

Professor Minan Lu, Department of Orthopedic Surgery, The Affiliated Hospital of Youjiang Medical University for Nationalities, 18 Zhongshan Second Road, Baise, Guangxi 533000, P.R. China
E-mail: 420966015@qq.com

*Contributed equally

Key words: osteosarcoma, stimulus-responsive, polymeric micelles, GNE-477, PI3K/Akt/mTOR cascade response

Introduction

Osteosarcoma (OS) is a malignant primary bone neoplasm that is most commonly diagnosed in children and adolescents and is the foremost cause of cancer-related mortality in young people (1,2). Standard treatment protocol for OS is based on resection surgery and polychemotherapy (3); however, the 5-year survival rate of patients with is typically <20% (4). Clinically, the residual OS cells following resection surgery may lead to continued bone destruction, new lesions in adjacent tissue and even potential recurrence of OS (5). On the other hand, conventional clinical chemotherapy agents often encounter challenges in accessing the tumor site to elicit therapeutic effects and their non-selective nature tends to engender strong toxicity to normal cells (6). Hence, there is need for the advancement of a novel, efficacious and low-toxicity treatment modality capable of precisely targeting tumor tissue to improve patient prognosis and quality of life.

Targeted therapies for OS have garnered interest, with small-molecule targeted inhibitors emerging as one of the most promising avenues (7). mTOR, a serine/threonine protein kinase, serves a pivotal role in regulating cell proliferation, differentiation, senescence and metabolism (8-10). Zhou *et al* (10) elucidated that the mTOR expression in OS tissue derived from 65 patients with primary OS exhibited

a positive correlation with progression of OS; inhibition of AKT/mTOR signaling has been reported to induce apoptosis in human OS cell line (11). Considering the association between mTOR and the occurrence and progression of OS, inhibitors targeting mTOR have become focal points of research and development by major pharmaceutical companies and scientific research institutions (12). GNE-477, a potent and efficacious dual PI3K/mTOR inhibitor capable of blocking both mTORC1 and mTORC2 signaling pathways (13), has shown encouraging outcomes in the treatment of numerous types of cancer, including renal cell carcinoma (14) and glioblastoma (15). Nevertheless, clinical utilization of mTOR inhibitors has not yielded substantial benefits for patients and causes severe adverse reactions and side effects. This primarily stems from inadequate tissue selectivity of mTOR inhibitors, with dosage tolerance and drug toxicity limiting development and use (16). While GNE-477 possesses promising potential in OS treatment, control over dosage, delivery system and application protocol are important for future clinical use. Consequently, there is need to develop a novel drug delivery system with good biocompatibility.

Stimulus-responsive self-assembled polymer micelles, capable of selectively delivering bioactive substances to specific sites within an organism, represent one of the research hotspots of controlled drug release systems (17). The underlying principle of stimulus-responsive drug carriers involves encapsulating or bonding hydrophobic drugs within stimulus-responsive polymers during the self-assembly process to form drug-loaded nano micelles. These micelles are modified and spliced with biologically recognizable moieties, which improve drug solubility in water, extend circulation time in the bloodstream, and achieve target-controlled release of drugs, thereby enhancing the therapeutic efficacy while decreasing systemic toxicity (18). External or physiological environmental stimuli are triggers for drug release, including light, temperature, ultrasound, magnetic force, enzymes, pH and redox substances (19-22). Reactive oxygen species (ROS), comprising OH^-, H_2O_2 and O_2^-, among others, are a class of free radicals in cells (23) that are highly released under disease conditions, particularly at sites of inflammation (24) and tumor advancement (25,26). Among ROS, H_2O_2 boasts an extended biological lifespan and facile diffusion both within and between cells (27). Moreover, oxidative stress caused by H_2O_2 is implicated in the pathogenesis of diverse types of disease, such as cancer, Parkinson's disease, cardiovascular disease (28). Therefore, the development of H_2O_2 stimulus-responsive biomaterials holds promise in decreasing drug toxicity for lesions characterized by heightened oxidative stress.

A variety of polymers are currently undergoing pre-clinical scrutiny to investigate potential in micelle formation, carrying chemotherapeutic agents, and anti-tumor effects in both *in vitro* cell experiments and *in vivo* animal models (29-32). Several polymeric micelles have progressed to clinical trials and have proved their efficacy in human subjects (33,34). Notably, GNE-477 has special amino and methanesulfonyl (Fig. 1A) groups, which facilitate its chemical synthesis and modification into a micellar structure. Among H_2O_2-sensitive moieties, phenylborate ester (PBAE) with readily modifiable structure and excellent biocompatibility represents one of the most sensitive structures to H_2O_2 (35). Under the induction of H_2O_2, the carbon-boron bond undergoes oxidative cleavage, leading to irreversible decomposition of PBAE (36). Additionally, dodecanoic acid (DA) functions as a graft-reactive monomer, while dextran (DEX) is hydrophobically modified to self-assemble into nano micelles featuring a shell-core structure. The combination of the aforementioned components as drug carriers holds promise in addressing the limitations associated with current antitumor medications. Thus, the present study synthesized GNE-477-loaded H_2O_2 stimulus-responsive dodecanoic acid-PBAE-dextran (DA-B-DEX) polymeric micelles (GNE-477@DBD) to release the drug in response to high H_2O_2 concentration in physiological lesion tissue and the anti-tumor effect of GNE-477@DBD against OS was investigated *in vitro* and *in vivo*.

Materials and methods

Cell culture. The human osteoblast cell line hFOB1.19 and OS cell lines MG-63, U2OS, and 143B were procured from iCell Bioscience, Inc. Cells were cultured in Dulbecco's Modified Eagle Medium/F-12 (DMEM-F12), supplemented with 10% FBS (both Gibco; Thermo Fisher Scientific, Inc.), 100 U/ml penicillin and 100 μg/ml streptomycin, under a 5% CO_2 atmosphere at 37˚C.

Animals. A total of 20 eight-week-old male BALB/c nude mice (weighted 18-20 g) were obtained from SPF (Beijing) Biotechnology Co., Ltd. and acclimatized for 1 week. The mice were housed at constant room temperature (60-65% humidity, 23±2˚C) with a 12/12-h light/dark cycle and free access to standard chow and water. The research protocol received approval from the Medical Ethics Committee of the First People's Hospital of Nanning (Guangxi, China; approval no. 2021-076-01) and complied with the guidelines of the National Institutes of Health Animal Care and Use Committee (37).

Synthesis and characterization of DA-B-DEX polymer. A total of 700.00 4-hydroxymethyl PBAE, 946.25 DA, 76.95 4-dimethylaminopyridine (DMAP), 733.32 1-ethyl-3-(3-dimethylaminopropyl)carbodiimide and 79.67 mg triethylamine were weighed and dissolved in 10 ml of dichloromethane and nitrogen was injected using a syringe to protect the system. Following 18 h reaction at room temperature, DA-B was obtained. A total of 700.00 DA-B, 761.32 $NaIO_4$ 190.40 mg and NH_4Cl (was dissolved in acetone (10 ml), with an equivalent volume of water. The reaction mixture was refluxed at 60˚C overnight, resulting in the synthesis of terminal hydroxylated DA-B. The hydroxylated DA-B (30 mg) was reacted with DEX (115.18 mg) under 4A molecular sieve (200 mg) and nitrogen protection at 60˚C for 60 h. The molecular sieve was removed via filtration and the filtrate was slowly dripped into ice-cold ethanol. A white precipitate emerged, which underwent centrifugation at 1,006 x g for 5 min at room temperature. The upper layer was discarded, and the ice-cold ethanol was added, followed by centrifugation at 1,006 x g for 3 min at room temperature. After being washed three times in ethanol, the precipitate yielded the DA-B-DEX polymer. The synthetic route of the DA-B-DEX polymer is shown in Fig. 1B.

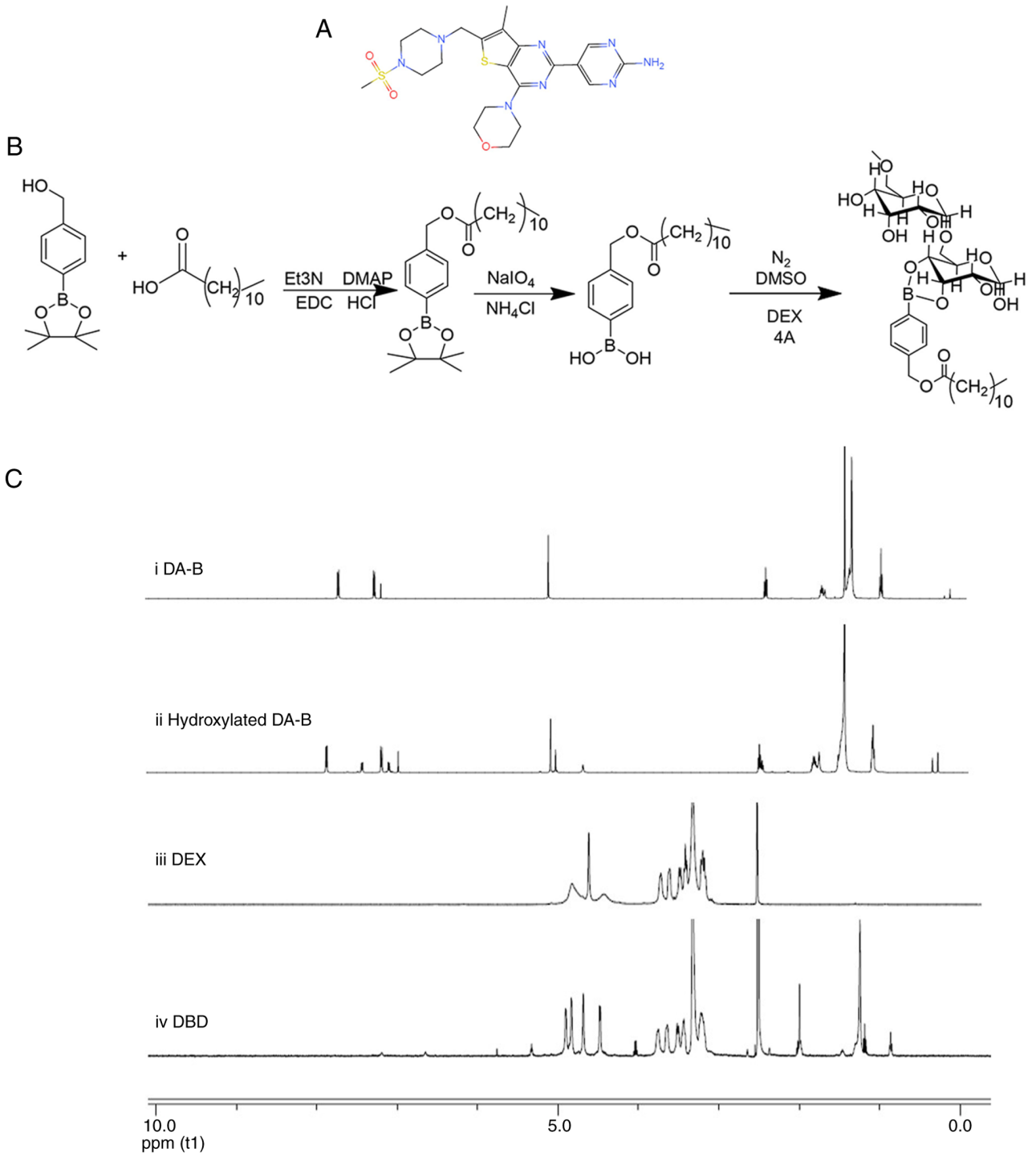

Figure 1. Synthesis and characterization of nano-drug delivery system. (A) Chemical structure of GNE-477. (B) Synthesis route for DBD polymeric micelles. (C) ^{1}H nuclear magnetic resonance spectra of i) DA-B, ii) hydroxylated DA-B, iii) DEX and iv) DBD. DBD, dodecanoic acid-phenylborate ester-dextran; DA-B, dodecanoic acid-phenylborate ester.

^{1}H nuclear magnetic resonance spectra of the DA-B-DEX polymers were determined at room temperature using a Nuclear Magnetic Resonance Spectrometer (Bruker), with deuterium oxide (D_2O) serving as the solvent and trimethylsilane (TMS) as the internal standard, and the reaction grafting rates were calculated based on the characteristic proton peaks (38). In the spectrum of hydrogen, the ratio of the area of hydrogen peaks at specific positions on the grafting group to the area of hydrogen peaks at certain characteristic positions on the main chain is termed as the grafting rates.

Synthesis of DA-B-DEX micelles and determination of critical micelle concentration (CMC). A total of 100 mg of the DA-B-DEX polymer was dissolved in ultra-pure water. Dialysis bags with a molecular weight cut-off of 3,500 KD were used for dialysis in ultra-pure water for 48 h, with the water refreshed every 4 h. Then, the solution in the dialysis bag

was freeze-dried in a freeze-drying machine for 24 h to yield a white solid, designated DA-B-DEX micelles.

CMC was determined utilizing a pyrene fluorescent probe, as previously described (39). A total of 0.0051 g pyrene was dissolved in 25 ml methanol, yielding a $1.01x10^{-3}$ mol/l pyrene solution, which was diluted with methanol to $1.616x10^{-6}$ mol/l pyrene solution. The prepared $1.616x10^{-6}$ mol/l pyrene solution (150 μl) was transferred to 10 ml bottles, and the methanol was evaporated at 50˚C for 5 min. A total of 10 ml DA-B-DEX solution ($1x10^{-4}$, $1x10^{-3}$, $1x10^{-2}$, $1x10^{-1}$, 1, 10, 100 and 1,000 mg/ml) was added to each of the 10 ml bottles containing a trace amount of pyrene. The solution underwent ultrasound treatment in a 50˚C water bath for 30 min, followed by standing at room temperature for 2 h. The fluorescence spectra of each solution were prepared for analysis by fluorescence photometer. The fluorescence photometer was set with a slit of excitation and emission at 5 nm, with a scanning range of 300-360 nm and an emission wavelength of 372 nm. The intensity of the emitted light at 333 (I333) and 339 nm (I339) excitation wavelengths were measured, regression curves were plotted, and the ratio of I339/I333 was calculated. The intersection of the two regression curves was calculated.

Preparation of GNE-477@DBD. A total of 91.5 DA-B-DEX and 8.5 mg GNE-477 (8.5 was co-dissolved and added to PBS buffer (100 ml). The resulting solution was then transferred to a dialysis bag with an interception relative molecular weight of 3,500 kDa and underwent dialysis in ultra-pure water for 48 h, with the water changed every 4 h. The suspension was filtered using 5.00 and 0.45 μm syringe filters and freeze-dried (Labconco Freezone 6), yielding a white powder named GNE-477@DBD.

Evaluation of micelle morphology and particle size distribution. To evaluate the morphological characteristics of GNE-477@DBD, samples were dropped onto a copper grid and negatively stained at room temperature for 2 min using 2% UO_2 acetate aqueous solution. Following drying, morphology was observed under a transmission electron microscope (TEM; FEI Talos F200S; Thermo Fisher Scientific, Inc.). Additionally, particle size distribution was determined by a laser particle sizer (Zetasizer Nano ZS ZEN3600, Malvern Instruments, Ltd.).

Drug release of GNE-477@DBD. The prepared drug-loaded micelles were dissolved in the following solutions: i) Pure PBS (pH=7.4), PBS solution containing ii) 10 or iii) 50 μmol/l H_2O_2; iv) simulated body fluid (SBF, pH=7.4) and v) simulated tumor microenvironment (pH=6.5, 100 μM H_2O_2). These solutions were sealed in dialysis bags with a cut-off relative molecular weight of 3,500 kDa and dialyzed for 50 h in 3,000 ml PBS buffer at 37˚C. A total of 1 ml GNE-477@DBD sample was taken and replaced with 1 ml fresh PBS solution to maintain solution volume. The released GNE-477 was quantified using high-performance liquid chromatography (HPLC; Agilent 1260, Agilent Technologies, Inc.). GNE-477 were filtered using 0.2 μm cellulose acetate filters and analyzed using an Eclipse XDB-C18 column (150.0x4.6 mm; 5 μm particle size) operated at 25˚C. The mobile phase consisted of 2% (v/v) acetic acid in water (mobile phase A) and 0.5% acetic acid in water and acetonitrile (10:90 v/v) (mobile phase B), and at a flow rate of 1.0 ml/min. The injection volume was 10 μl and the wavelength of the UV detector is set at 280 nm. The quantification was performed by applying the standard calibration curve.

In vitro uptake of GNE-477@DBD. The uptake of GNE-477@DBD was assessed in MG-63, U2OS and 143B cell lines following 2 and 6 h incubation. Cells were seeded in a 2-multiwell plate at a density of $2x10^4$ cells/well (2 ml/well) and cultured in DMEM for 24 h at 37˚C and 5% CO_2. Culture medium was replaced with a dispersion of GNE-477@DBD in fresh DMEM (0.25 mg/ml, 1 ml/well), and the cells were incubated for 2 or 6 h at room temperature. Upon reaching ~90% confluence, cells were treated with Nile Red (HY-D0718, MedChemExpress)-loaded GNE-477 for 1 h at room temperature, fixed and stained with DAPI for 10 min at room temperature using the method described previously (40). Finally, the slides were analyzed using a Leica TCS SP8 confocal laser scanning microscope (Leica-Microsystems GmbH). Nile Red was excited with a 560 nm laser and emission was collected at 570-620 nm (41).

MTT assay. hFOB1.19, MG-63, U2OS and 143B cells were cultured in a complete RPMI-1640 medium supplemented with 10% FBS, 100 IU/ml penicillin and 100 mg/ml streptomycin (all Gibco; Thermo Fisher Scientific, Inc.). The cells were seeded in 96-well plates ($2x10^4$ cells/well) and incubated overnight at 37˚C and 5% CO_2. At 24, 48 and 72 h, 10 μl MTT solution (Wuhan Biofavor Biotechnology Service Co., Ltd.) was added for 4 h at room temperature and the medium was removed. The formazan crystals were dissolved in 150 μl DMSO. Blank wells were used as blank groups. The optical density (OD) at 560 nm was measured by a microplate reader. Finally, the cell viability was calculated as follows: Cell viability (%)=OD of treated cells/OD of control x100. The experiment was repeated three times.

Flow cytometry. The apoptotic rate (early + late apoptosis) and cell cycle distribution were assessed using flow cytometry. For apoptosis assessment, MG-63, U2OS and 143B cells subjected to different treatments (Control, GNE-477, DBD, and GNE-477@DBD) were suspended in binding buffer and incubated with 5 Annexin V-FITC and 10 μl propidine iodide (PI; BD Biosciences) for 15 min at room temperature away from light. The apoptotic cells were determined on an Attune™ NxT flow cytometer (Thermo Fisher Scientific, Inc.), and results were analyzed using FlowJo software (version 9.3.2; FlowJo LLC). For cell cycle distribution, cells were fixed in 75% ethanol for 2 h at 4˚C and treated with RNase A for 40 min at room temperature. Staining with PI for 40 min at room temperature, followed by detection on an Attune™ NxT flow cytometer (Thermo Fisher Scientific, Inc.), and Attune NxT Software (version 3.2.1; Thermo Fisher Scientific, Inc.) to determine the percentage of cells in G0/G1, S and G2/M phases.

Western blotting. Protein samples were extracted from OS cells or tissue using RIPA buffer (BioTeke Corporation), and the protein content was measured using a BCA protein

quantification kit (Beyotime Institute of Biotechnology). 10 μg of protein from each sample was loaded and separated by 10% SDS-PAGE (Sinopharm Chemical Reagent Co., Ltd.), followed by transfer onto PVDF membranes. The membrane was blocked with 5% skimmed milk in Tris-buffered saline at room temperature for 1 h, followed by overnight incubation at 4˚C with primary antibodies (all Cell Signaling Technology, Inc.) against caspase 3 (1:1,000; cat. no. 9662), cleaved-caspase 3 (1:1,000; cat. no. 9661), Bax (1:1,000; cat. no. 2772), Bcl-2 (1:1,000; cat. no. 15071), Cyclin D1 (1:1,000; cat. no. 2922), Cyclin E (1:1,000; cat. no. 20808), AKT (1:1,000; cat. no. 9272), phosphorylated-AKT (p-AKT; 1:500; cat. no. 9271), mTOR (1:1,000; cat. no. 2972), p-mTOR (1:1,000; cat. no. 2971) and GAPDH (1:1,000; cat. no. 2118). After washing by TBST (Tris-buffered saline with 0.1% Tween 20), the membrane was incubated with horseradish peroxidase-conjugated goat anti-rabbit secondary antibodies (Abcam; 1:10,000; cat. no. ab205718) for 2 h at room temperature. Protein bands were visualized using enhanced chemiluminescence reagent (Thermo Fisher Scientific, Inc.) and semi-quantification was performed using Image J software (version 1.54i 03; National Institutes of Health).

Reverse transcription-quantitative (RT-q) PCR. Total RNA from OS cell lines was isolated using TRIzol (Invitrogen; Thermo Fisher Scientific, Inc.), followed by RT into cDNA using PrimeScript™ RT reagent kit (TransGen Biotech Co., Ltd.), according to the manufacturer's protocol. Next, qPCR was performed using AceQ qPCR SYBR Green Master Mix (MedChemExpress LLC). The analysis of mRNA expression levels was conducted by the $2^{-\Delta\Delta Cq}$ method (42), with GAPDH as the internal reference. The sequences of the primers were as follows: Caspase 3, forward, 5'-CGTGCTTCTAAGCCATGGTG-3' and reverse, 5'-GTCCCACTGTCCGTCTCAAT-3'; Bax, forward, 5'-TGCCTCAGGATGCATCTACC-3' and reverse, 5'-AAGTAGAAAAGCGCGACCAC-3'; Bcl-2, forward, 5'-AGGGCATTCAGTGACCTGAC-3' and reverse, 5'-CGATCCGACTCACCAATACC-3'; Cyclin D1, forward, 5'-ACCCGACGAGTTACTGCAAAT-3' and reverse, 5'-TCTGTTTGGTGTCCTCTGCC-3'; Cyclin E, forward, 5'-AGAGGAAGGCAAACGTGACC-3' and reverse, 5'-TATTGTCCCAAGGCTGGCTC-3' and GAPDH, forward, 5'-AGGCCGGTGCTGAGTATGTC-3' and reverse, 5'-TGCCTGCTTCACCACCTTCT-3'. The thermocycling conditions were as follows: Initial denaturation at 96˚C for 5 min, followed by 40 cycles of 95˚C for 30 sec and 68˚C for 20 sec.

Xenograft model. U2OS tumor-bearing Balb/c mice were generated by subcutaneously injecting U2OS cells ($2x10^6$/mouse). Then, the mice were randomly divided into four groups (n=5/group) as follows; Control, GNE-477, DBD and GNE-477@DBD. Every 2 days, the state of the mice was observed and the body weight was determined. In addition, the tumor size was measured using vernier calipers and tumor volume was calculated as follows: Tumor volume=0.5x length x width^2. Once the inoculated tumor volume reached 100-200 mm^3, 25 mg/kg GNE-477, DBD@GNE-477 (containing 25 mg/kg GNE-477), or an equivalent volume of vehicle control (DBD) and negative control (PBS) were administered intraperitoneally. Weight loss ≥20% within a short period or the average tumor diameter exceeds 20 mm, the experiment was terminated and mice were euthanized. Mice were anesthetized after 34 days using 3% isoflurane and then euthanized by cervical dislocation. Cessation of heartbeat and breathing were considered to confirm death. The heart, liver, spleen, lung, kidney and tumor were removed, washed with saline, weighed, and fixed for 24 h at 4 ˚C in 4% formaldehyde for subsequent staining.

Hematoxylin and eosin (H&E) staining. To evaluate the potential side effects of drugs on organs, H&E staining was performed. The fixed heart, liver, spleen, lung and kidney tissue was dehydrated, embedded in paraffin and cut into 4 μm-sections. Thereafter, the samples were stained with hematoxylin (Beijing Solarbio Science & Technology Co., Ltd.) for 8 min at room temperature and rinsed with running water. Samples were differentiated with 5% acetic acid for 1 min, washed with running water for 10 min, stained with eosin (Beijing Solarbio Science & Technology Co., Ltd.) for 1 min at room temperature, and rinsed three times with running water for 5 min. Finally, the images were captured under a light microscope (magnification, x100).

Statistical analysis. All data are presented as the mean ± SD. GraphPad PRISM 8.0 software (Dotmatics) was used for statistical analysis by one- or two-way ANOVA followed by Tukey's post hoc test. Each sample was evaluated in a minimum of three experimental replicates. $P<0.05$ was considered to indicate a statistically significant difference.

Results

Characterization of DA-B-DEX polymer. The ^{1}H-nuclear magnetic resonance (NMR) spectra of DA-B, hydroxylated DA-B, DEX and DA-B-DEX conjugates are shown in Fig. 1C. In the spectrum of DA-B, the characteristic single peak of pinacol ester (1.24 ppm) and the two characteristic peaks of benzene rings were clearly discernible. The chromatogram of hydroxylated DA-B exhibited disappearance of the single peak at 1.24 ppm, confirming the removal of the protective group (pinacol ester). Hydroxylated DA-B was successfully grafted onto DEX, yielding a calculated grafting rate of ~3% (Fig. 1C), meeting the general requirements for formation of amphiphilic micelles (grafting rate <10%, ensuring the solubility of the micelles) (43).

Preparation and release of GNE-477@DBD. As in Fig. 2A, the intersection of the two regression curves for the I339/I333 ratio of DA-B-DEX pyrene solution was at (-1.828,0.5965). CMC of DA-B-DEX micelles was 0.01486 mg/ml; the low CMC signified that DA-B-DEX readily formed micelles and maintained the core-shell structure under highly diluted conditions. The degradation process of DA-B-DEX micelles is shown in Fig. 2B. In the absence of H_2O_2, almost all drug-loaded micelles were spherical and intact, whereas exposure to 100 μmol/l H_2O_2 resulted in notable disruption of micelle structure, accompanied by an alteration in the particle size distribution of the micelles towards inhomogeneous (Fig. 2C). The *in vitro* release profile of GNE-477 revealed a significant disparity in drug release from DA-B-DEX in PBS, 10 and 50 μmol/l H_2O_2

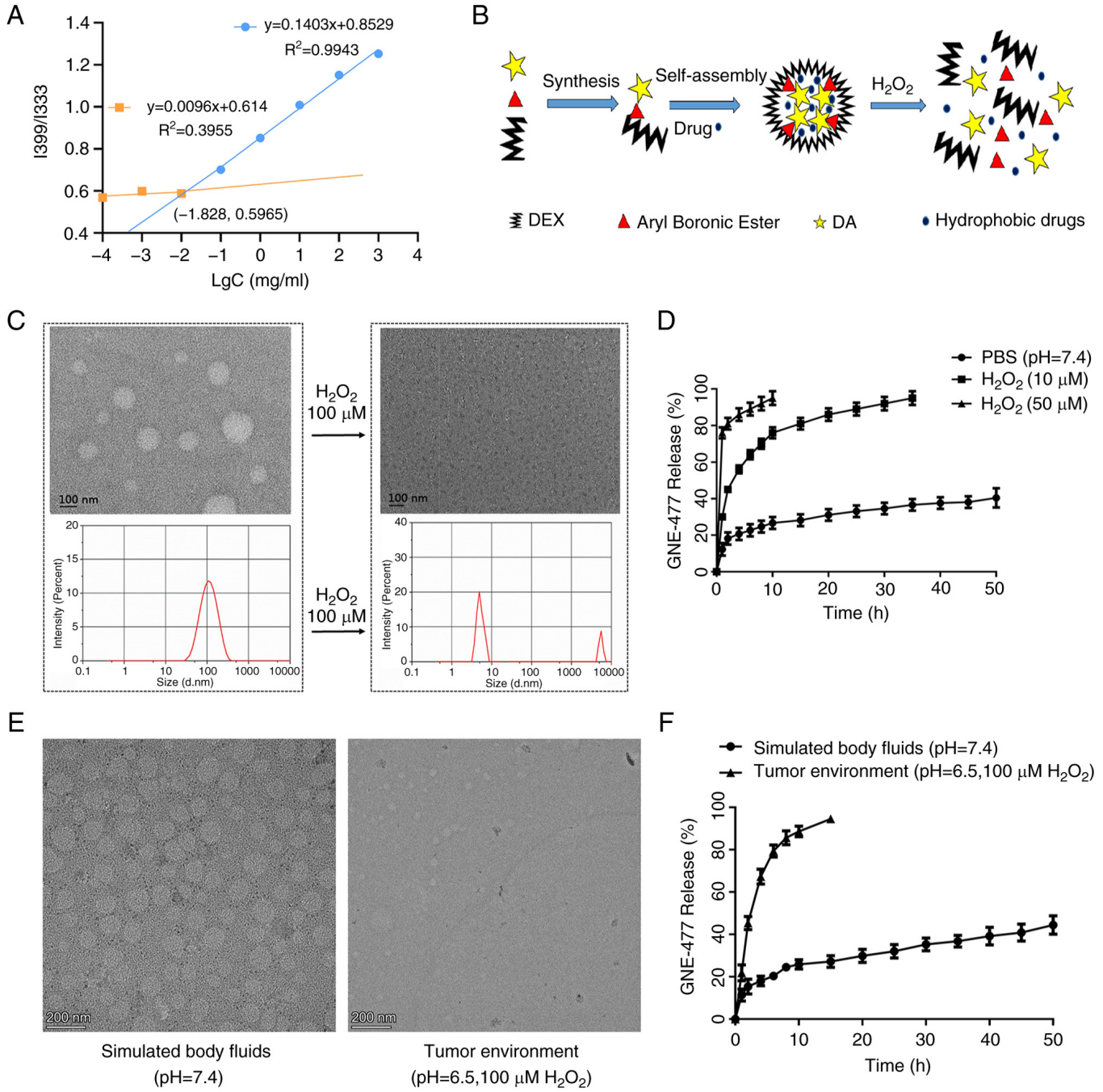

Figure 2. Preparation and drug release of GNE-477@DBD. (A) Fluorescence intensity (I339/I333) ratio of pyrene as a function of logarithmic DBD concentration. (B) Degradation of DBD. (C) Morphology and particle size of GNE-477@DBD determined by TEM in the presence or absence of 100 μM H_2O_2 treatment. (D) Drug release rate of GNE-477@DBD in PBS. (E) Morphology of GNE-477@DBD determined by TEM. (F) Drug release rate. DBD, dodecanoic acid-phenylborate ester-dextran; TEM, transmission electron microscope.

environments. At 2 h, drug release in the PBS group was 20%, while it reached 41 and 85% at 10 and 50 μmol/l H_2O_2, respectively (Fig. 2D). TEM was conducted to assess rupture and release of GNE-477@DBD under conditions of SBF (pH=7.4) and tumor environment (pH=6.5, 100 μM H_2O_2). The micellar structure of GNE-477@DBD was more susceptible to disruption in the tumor environment (Fig. 2E), exhibiting a higher drug release rate compared with SBF (Fig. 2F). These findings indicated that the DA-B-DEX micelles ruptured and released the drug faster in the presence of H_2O_2, thus DA-B-DEX micelles were H_2O_2-responsive.

Effect of GNE-477@DBD on drug uptake of OS cells in vitro. Following 2 h incubation, free GNE-477 was distributed in both cytoplasm and nucleus, while in the GNE-477@DBD group, GNE-477 was predominantly located in the cytoplasm, exhibiting a weaker fluorescence intensity compared with the GNE-477 group. Following 6 h incubation, the fluorescence intensity of GNE-477 in the GNE-477@DBD group notably increased, indicating a progressive internalization of more GNE-477@DBD into the cells, followed by sustained release of GNE-477 in the cells (Fig. 3A-C).

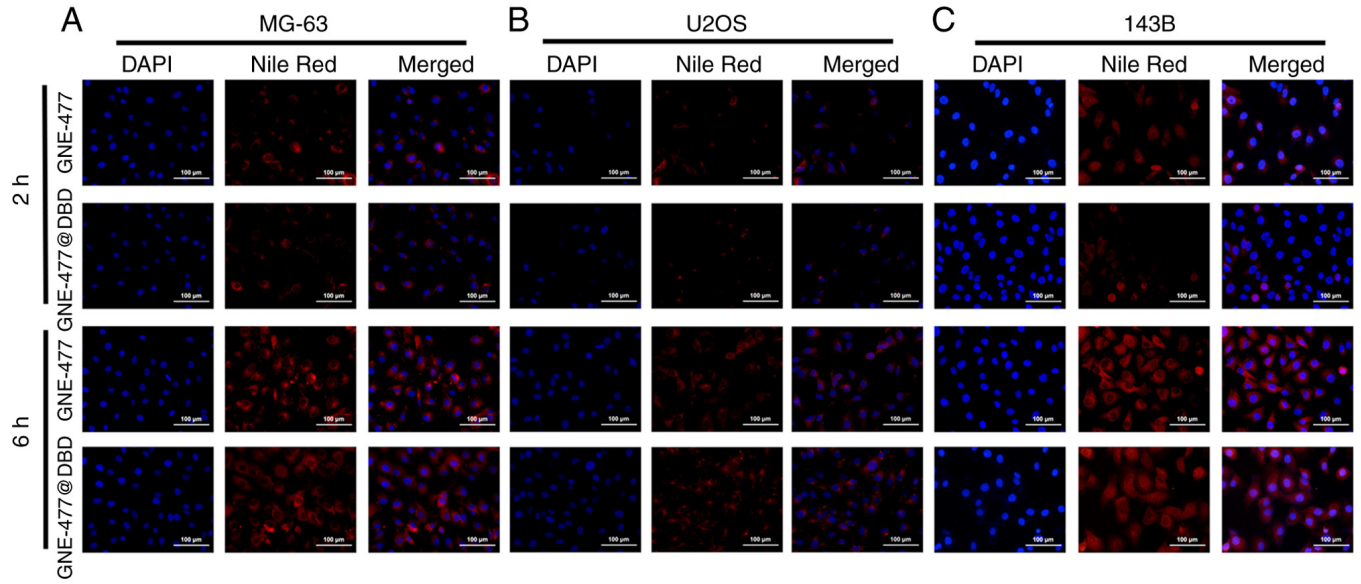

Figure 3. Cellular uptake of GNE-477@DBD in analyzed by fluorescent tracer technique. (A) MG-63, (B) U2OS and (C) 143B cells. DBD, dodecanoic acid-phenylborate ester-dextran.

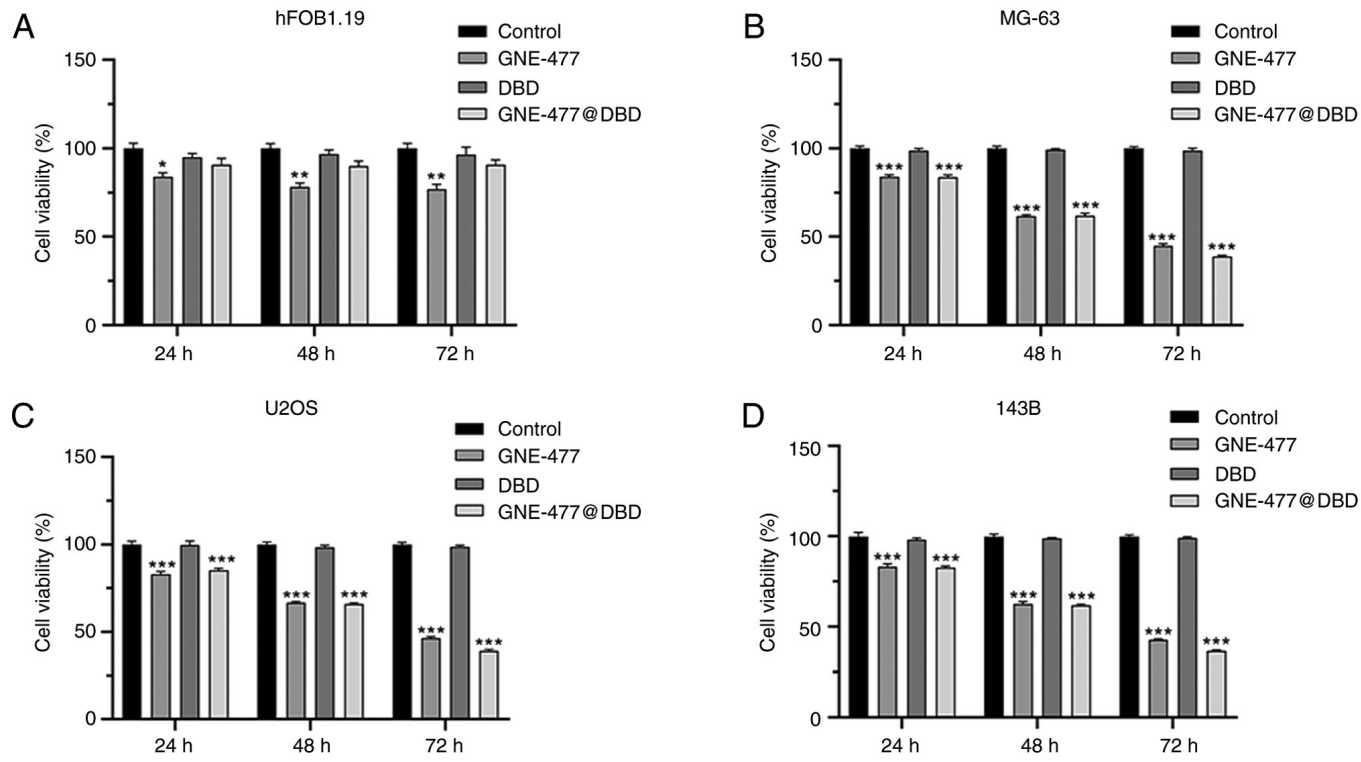

Figure 4. Cytotoxic effects of GNE-477@DBD on normal and osteosarcoma cell lines. (A) hFOB1.19, (B) MG-63, (C) U2OS and (D) 143B cells. *P<0.05, **P<0.01 and ***P<0.001 vs. Control. DBD, dodecanoic acid-phenylborate ester-dextran.

Effect of GNE-477@DBD on viability, apoptosis and cell cycle of OS cells in vitro. Normal human osteoblast hFOB1.19 and MG-63, U2OS and 143B OS cells were treated with PBS, GNE-477, DBD and GNE-477@DBD for 24, 48, and 72 h. The findings revealed that DBD and GNE-477@DBD exhibited good biocompatibility and low toxicity to normal cells (Fig. 4A) and both GNE-477 and GNE-477@DBD demonstrated inhibitory effects on OS cell viability (Fig. 4B-D). Following 24 h drug treatment, flow cytometry showed that compared with Control, both GNE-477 and GNE-477@DBD induced apoptosis in OS cell lines (Fig. 5) and elevated the proportion of cells in G1 phase, suggesting that GNE-477 and GNE-477@DBD blocked cell division at G1 phase and prevented cell cycle progression (Fig. 6). Furthermore, protein and mRNA levels of cell apoptosis- and cell cycle-associated genes were verified by western blot and RT-qPCR in U2OS cells (Fig. 7A and B). Following 24 h drug treatment, compared with the Control group, the expression of Bcl-2 and cyclin D1 and E protein

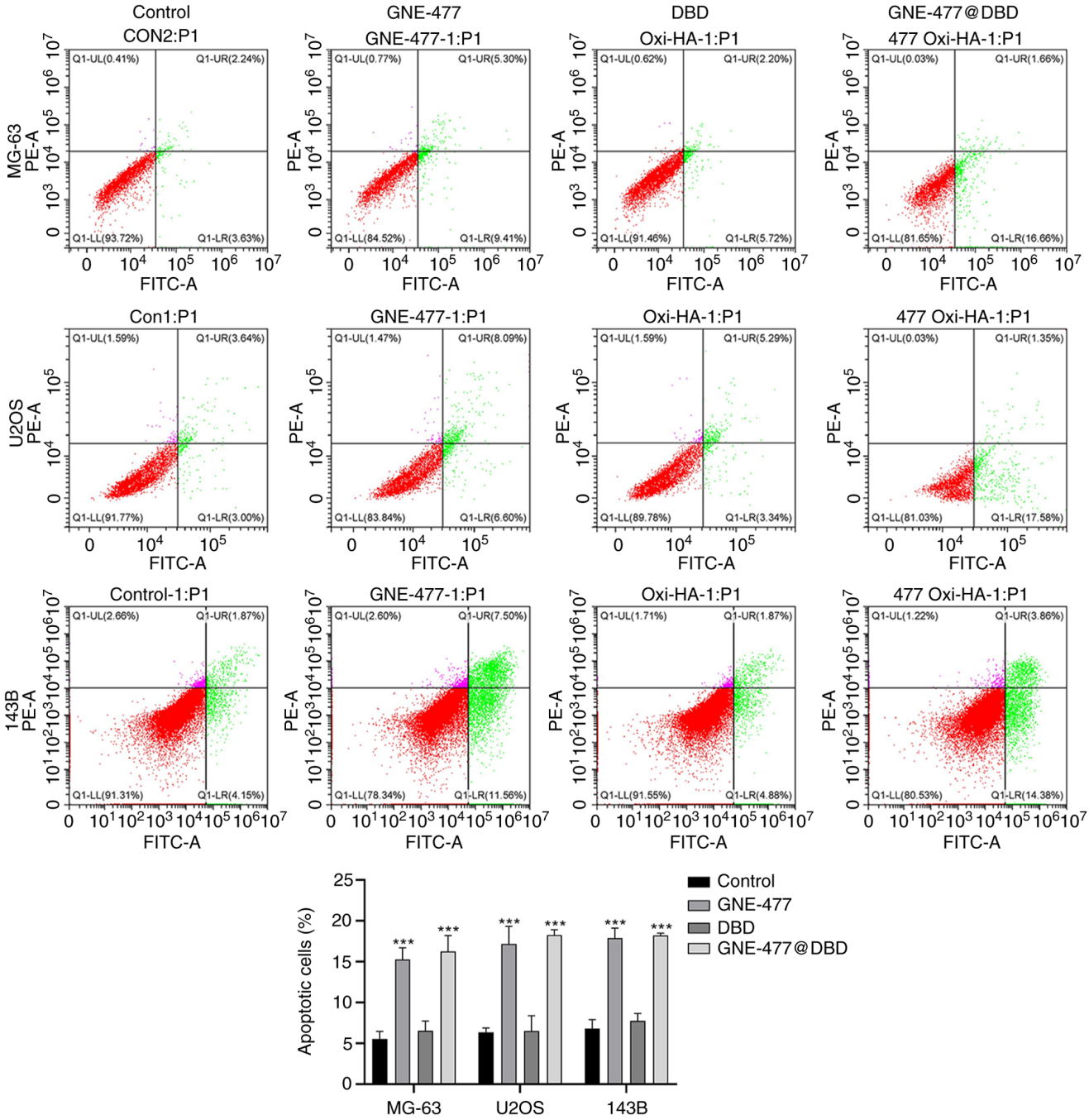

Figure 5. Effect of GNE-477@DBD on apoptosis of osteosarcoma cell lines detected by flow cytometry. ***P<0.001 vs. Control. DBD, dodecanoic acid-phenylborate ester-dextran.

and mRNA was downregulated, while Bax and caspase 3 protein and mRNA expression levels were upregulated in the GNE-477 and GNE-477@DBD groups, indicating that GNE-477 exerted anti-tumor effects following encapsulation in H_2O_2-responsive nano micelles. Additionally, western blot analysis revealed that GNE-477 and GNE-477@DBD inhibited expression of proteins involved in the Akt/mTOR cascade response, confirmed by Akt agonist treatment (Fig. 7C).

Anti-OS activity and biosafety of GNE-477@DBD in vivo. A nude mouse model was established to evaluate *in vivo* anti-tumor ability of GNE-477@DBD. GNE-477 and DBD@GEN-477 groups demonstrated tumor regression and impeded tumor growth compared with the Control group, notably, the anti-tumor efficacy of GNE-477@DBD surpassed that of free GNE-477 (Fig. 8A and B). There were no significant differences in the body weight of mice between groups, thereby indicating the safety profile of this nanoscale drug delivery system (Fig. 8C). Moreover, western blot results corroborated that protein expression of p-AKT, p-mTOR, Bcl-2 and cyclin D1 and E decreased in the GNE-477 and GNE-477@DBD groups, while protein expression of Bax and cleaved-caspase 3 increased. These results suggested that treatment with GNE-477 and GNE-477@DBD suppressed PI3K/AKT/mTOR pathway activation and facilitated apoptosis of tumor cells (Fig. 8D). Histopathological examination

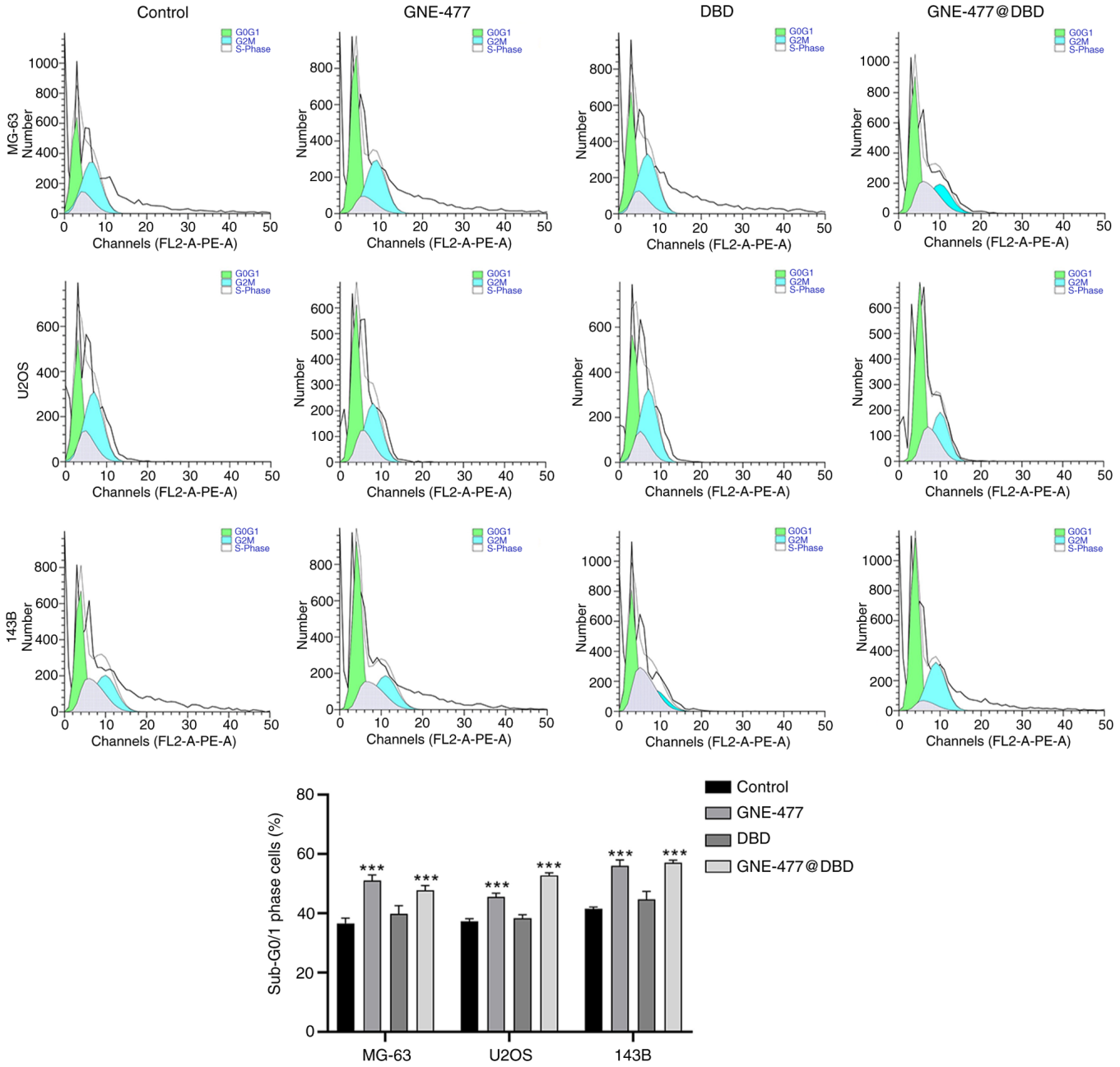

Figure 6. Effect of GNE-477@DBD on cell cycle progression of osteosarcoma cell lines detected by flow cytometry. ***P<0.001 vs. Control. DBD, dodecanoic acid-phenylborate ester-dextran.

of major organs stained with H&E demonstrated varying degrees of damage in the GNE-477 group, whereas both the DBD and GNE-477@DBD groups exhibited no discernible organ damage, indicating that DBD nano micelles had favorable biocompatibility and mitigated organ damage caused by GNE-477 (Fig. 9).

Discussion

OS is widely acknowledged as the most prevalent type of primary bone malignancy, yet conventional chemotherapy drugs often carry deleterious side effects and lack targeted ability, compromising the prognosis and quality of life for patients (44). Biomaterials have shown promising potential in the treatment of bone-associated disease, such as the deterioration of human dental enamel, tooth regeneration and bone tissue repair (45-47). Consequently, development and application of drug delivery systems hold promise for enhancing the treatment of OS (48). The design of nanoplatforms for stable delivery of hydrophobic anticancer drugs, offering versatility and precision, has garnered increasing attention (49,50). Here, an H_2O_2-responsive DA-B-DEX polymeric micelles loading GNE-477 system was engineered, demonstrating not only the therapeutic effect of GNE-477 against OS but also improved drug uptake and targeted efficacy in both *in vitro* and *in vivo* settings.

The GNE-477-loaded DA-B-DEX delivery system presents supplementary benefits compared with systemic administration of GNE-477 for OS treatment. PBAE, serving as the H_2O_2 recognition group, triggers degradation following

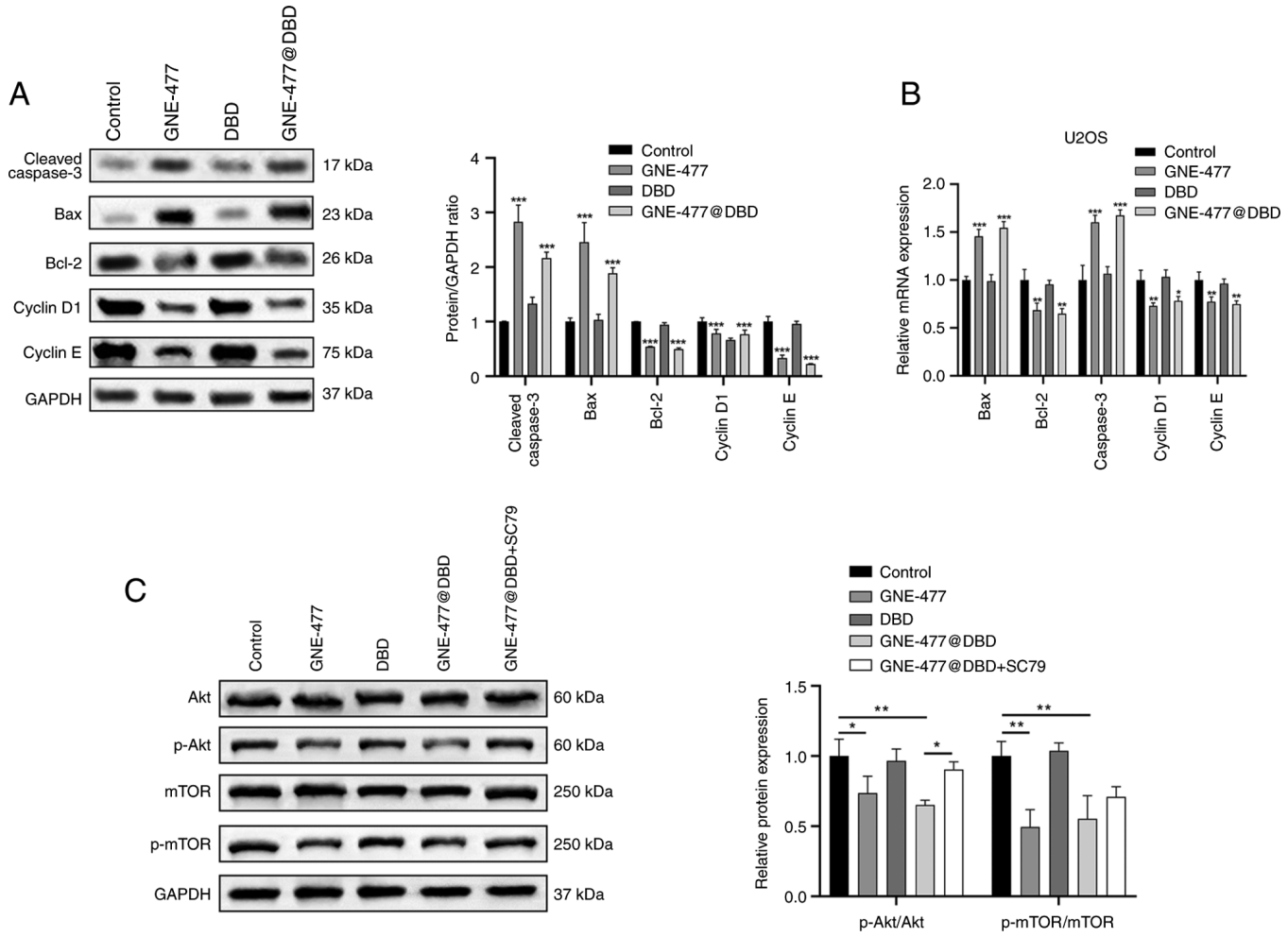

Figure 7. Effect of GNE-477@DBD on protein and mRNA levels of genes associated with apoptosis, cell cycle and the Akt/mTOR cascade response in U2OS cells. (A) Western blot and (B) mRNA levels of apoptosis- and cell cycle-associated genes. (C) Western blot of Akt/mTOR cascade response-associated protein expression. *P<0.05, **P<0.01 and ***P<0.001 vs. Control. DBD, dodecanoic acid-phenylborate ester-dextran; p-, phosphorylated-.

its conversion to phenol upon exposure to high concentrations (100 μmol/l) of H_2O_2. The phenol undergoes a quinone dimethylformamide rearrangement, facilitating decomposition of the polyester main chain and expediting degradation process. In addition, the combination of PBAE, DA and DEX exhibits excellent synthetic feasibility and hydrolytic properties as a drug carrier micelle (51). The small molecules generated following its degradation are readily cleared by the body, allowing specific targeting and drug release to OS cells (52). Here, characterization indicated that DA-B-DEX drug-loaded micelles possessed advantages of low CMC, high loading efficiency, nanoscale diameter, good sensitivity and controlled release, suggesting their potential as a novel drug-targeted delivery system. Moreover, the significantly enhanced drug release rate and drug uptake rate corroborate the aforementioned results.

Nanodrug carriers not only augment therapeutic efficacy but also mitigate the toxic side effects during treatment, rendering them the focus of increased clinical endeavors for the development of novel drug carriers (53,54). Here, DBD and GNE-477@DBD exerted lower toxicity against normal cells, indicating the low toxicity and safety profile. In addition, the anti-tumor efficacy of GNE-477@DBD was validated both *in vitro* and *in vivo*. GNE-477@DBD inhibited tumor cell viability, arrested cell cycle in G1 phase and induced apoptosis. To investigate the *in vivo* anti-OS activity of GNE-477@DBD, a nude mouse tumor model was established via subcutaneous injection of U2OS cells. The *in vivo* outcomes illustrated that GNE-477 blocked the PI3K/Akt/mTOR cascade reaction of tumors *in vivo* and displayed notable anti-tumor effects, with GNE-477@DBD exhibiting more positive therapeutic effects compared with the GNE-477 group, with almost no side effect on organs. This was consistent with findings of Xu *et al* (5), who demonstrated that novel zoledronic acid-loaded hyaluronic acid/polyethylene glycol/nano-hydroxyapatite nanoparticles specifically inhibit proliferation of OS cells, while exerting negligible effects on normal cells. Moreover, the aforementioned study demonstrated that *in vivo* local administration of nanoparticles markedly augmented intratumoral vascular inflammation and facilitated tumor tissue necrosis and apoptosis. The present nanomaterial was H_2O_2-responsive, rendering it more sensitive and targeted.

The present study developed an amphiphilic H_2O_2-stimulated responsive DA-B-DEX nano micelles system for stable conveyance of hydrophobic anticancer drugs.

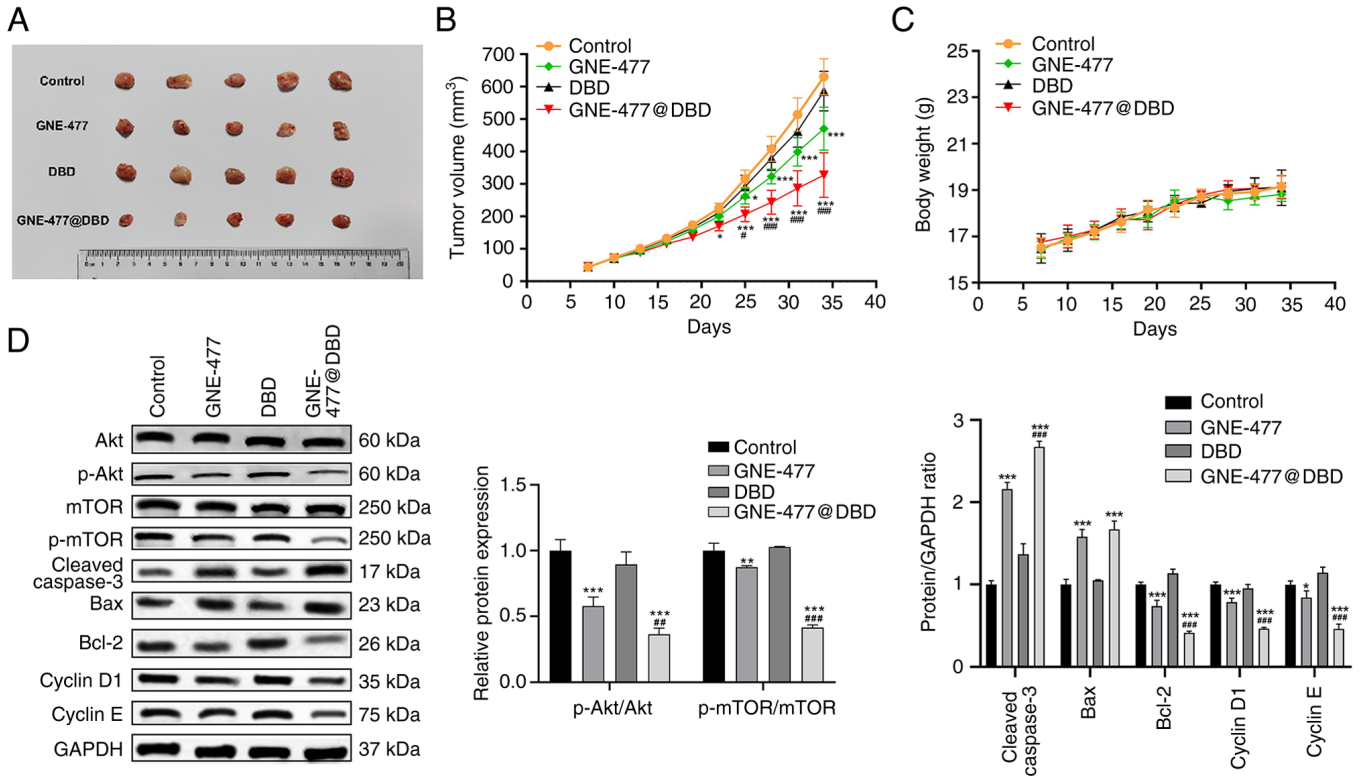

Figure 8. *In vivo* antitumor activity and safety evaluation of GNE-477@DBD. (A) Gross features of tumors. (B) Tumor volume curve. (C) Body weight curve. (D) Western blot of apoptosis-, cell cycle- and Akt/mTOR pathway-associated protein expression. *P<0.05, **P<0.01 and ***P<0.001 vs. Control; $^{\#}$P<0.05, $^{\#\#}$P<0.01, $^{\#\#\#}$P<0.001 vs. GNE-477. DBD, dodecanoic acid-phenylborate ester-dextran; p-, phosphorylated-.

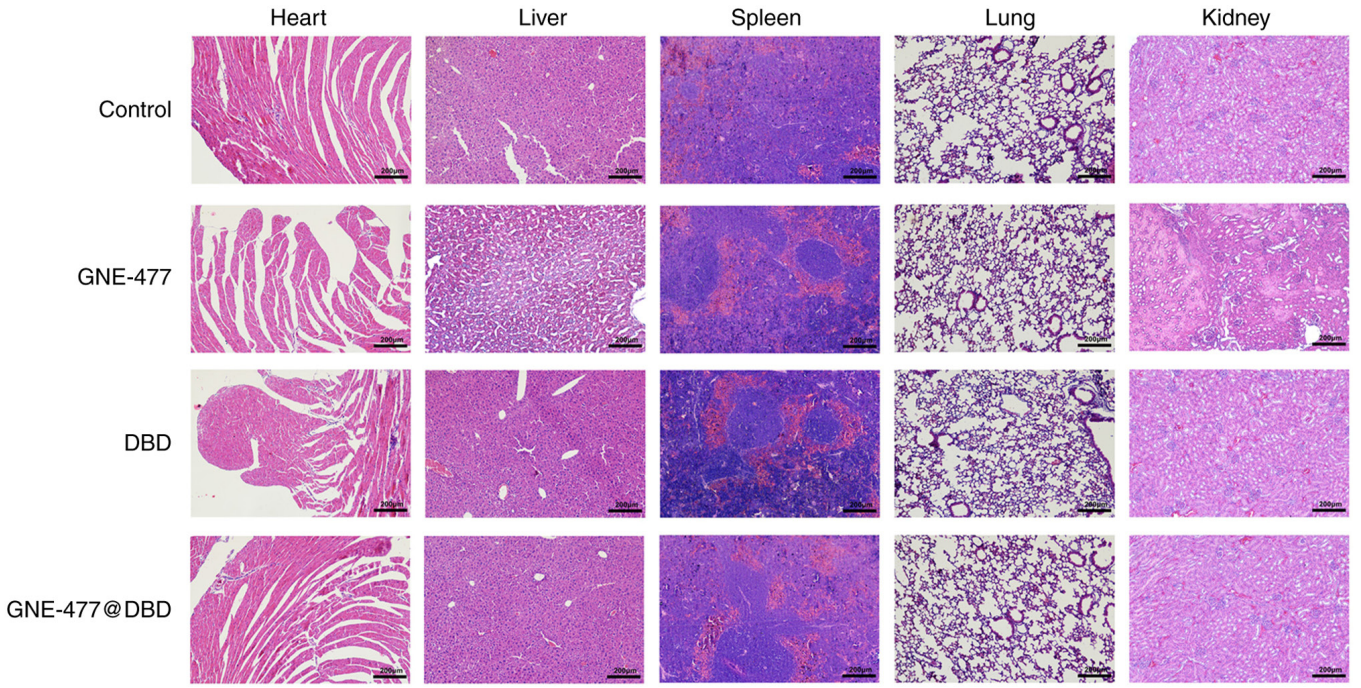

Figure 9. Hematoxylin and eosin staining of major organs. DBD, dodecanoic acid-phenylborate ester-dextran.

GNE-477@DBD nanomaterial demonstrated enhanced selectivity towards cancer cells in comparison with free drug and potent anticancer activity and biosafety *in vivo*. To the best of our knowledge, there is no prior report of application of DA-B-DEX polymeric micelles as carriers for anti-cancer drugs such as GNE-477. Further exploration of synergistic effects arising from the combination of GNE-477, a dual PI3K/mTOR inhibitor, with nanomaterial delivery systems holds promise in surmounting the limitations of GNE-477 in clinical applications.

Acknowledgements

Not applicable.

Funding

The present study was supported by Department of Education of Guangxi Zhuang Autonomous Region, Project of Enhancing the Basic Research Ability of Young Teachers in Colleges and Universities (grant no. 2021KY0105) and Nanning First People's Hospital Scientific Research and Technology Development Program Project (grant no. 2021001).

Availability of data and materials

The data generated in the present study may be requested from the corresponding author.

Authors' contributions

SP and ZZ conceived and designed the study and wrote the manuscript. XF and JW analyzed data. HL, YX and ZS performed the experiments. GL and GF interpreted data. ZH, RG and ML reviewed the manuscript and interpreted the data. YX analyzed the data and revised the manuscript. GL and GF confirmed the authenticity of all the raw data. All authors have read and approved the final manuscript.

Ethics approval and consent to participate

All animal experiments were approved by the Medical Ethics Committee of the First People's Hospital of Nanning (approval number: 2021-076-01). The study was reported in accordance with National Research Council's Guide for the Care and Use of Laboratory Animals ARRIVE guidelines (arriveguidelines.org) and Basel Declaration. The euthanasia method in this study was informed by the American Veterinary Medical Association Guidelines for the Euthanasia of Animals (2020).

Patient consent for publication

Not applicable.

Competing interests

The authors declare that they have no competing interests.

References

1. Smeland S, Bielack SS, Whelan J, Bernstein M, Hogendoorn P, Krailo MD, Gorlick R, Janeway KA, Ingleby FC, Anninga J, *et al*: Survival and prognosis with osteosarcoma: Outcomes in more than 2000 patients in the EURAMOS-1 (European and American Osteosarcoma Study) cohort. Eur J Cancer 109: 36-50, 2019.
2. Harrison DJ, Geller DS, Gill JD, Lewis VO and Gorlick R: Current and future therapeutic approaches for osteosarcoma. Expert Rev Anticancer Ther 18: 39-50, 2018.
3. Heymann MF, Brown HK and Heymann D: Drugs in early clinical development for the treatment of osteosarcoma. Expert Opin Investig Drugs 25: 1265-1280, 2016.
4. Anderson ME: Update on survival in osteosarcoma. Orthop Clin North Am 47: 283-292, 2016.
5. Xu Y, Qi J, Sun W, Zhong W and Wu H: Therapeutic effects of zoledronic Acid-loaded hyaluronic Acid/Polyethylene Glycol/Nano-Hydroxyapatite nanoparticles on osteosarcoma. Front Bioeng Biotechnol 10: 897641, 2022.
6. Zhao X, Wu Q, Gong X, Liu J and Ma Y: Osteosarcoma: A review of current and future therapeutic approaches. Biomed Eng Online 20: 24, 2021.
7. Liu J, Yao Q, Peng Y, Dong Z, Tang L, Su X, Liu L, Chen C, Ramalingam M and Cheng L: Identification of Small-molecule inhibitors for osteosarcoma targeted therapy: Synchronizing in silico, in vitro, and in vivo analyses. Front Bioeng Biotechnol 10: 921107, 2022.
8. Meng D, Frank AR and Jewell JL: mTOR signaling in stem and progenitor cells. Development 145: dev152595, 2018.
9. Costa RLB, Han HS and Gradishar WJ: Targeting the PI3K/AKT/mTOR pathway in triple-negative breast cancer: A review. Breast Cancer Res Treat 169: 397-406, 2018.
10. Zhou Q, Deng Z, Zhu Y, Long H, Zhang S and Zhao J: mTOR/p70S6K signal transduction pathway contributes to osteosarcoma progression and patients' prognosis. Med Oncol 27: 1239-1245, 2010.
11. Miwa S, Sugimoto N, Yamamoto N, Shirai T, Nishida H, Hayashi K, Kimura H, Takeuchi A, Igarashi K, Yachie A, *et al*: Caffeine induces apoptosis of osteosarcoma cells by inhibiting AKT/mTOR/S6K, NF-κB and MAPK pathways. Anticancer Res 32: 3643-3649, 2012.
12. Zhuo BB, Zhu LQ, Yao C, Wang XH, Li SX, Wang R, Li Y and Ling ZY: ADCK1 is a potential therapeutic target of osteosarcoma. Cell Death Dis 13: 954, 2022.
13. Heffron TP, Berry M, Castanedo G, Chang C, Chuckowree I, Dotson J, Folkes A, Gunzner J, Lesnick JD, Lewis C, *et al*: Identification of GNE-477, a potent and efficacious dual PI3K/mTOR inhibitor. Bioorg Med Chem Lett 20: 2408-2411, 2010.
14. Ye X, Ruan JW, Huang H, Huang WP, Zhang Y and Zhang F: PI3K-Akt-mTOR inhibition by GNE-477 inhibits renal cell carcinoma cell growth in vitro and in vivo. Aging (Albany NY) 12: 9489-9499, 2020.
15. Wang Y, Shen H, Sun Q, Zhao L, Liu H, Ye L, Xu Y, Cai J, Li Y, Gao L, *et al*: The new PI3K/mTOR inhibitor GNE-477 inhibits the malignant behavior of human glioblastoma cells. Front Pharmacol 12: 659511, 2021.
16. Barber NA and Ganti AK: Pulmonary toxicities from targeted therapies: A review. Target Oncol 6: 235-243, 2011.
17. Ulbrich K, Hola K, Subr V, Bakandritsos A, Tucek J and Zboril R: Targeted drug delivery with polymers and magnetic nanoparticles: Covalent and noncovalent approaches, release control, and clinical studies. Chem Rev 116: 5338-5431, 2016.
18. MacEwan SR, Callahan DJ and Chilkoti A: Stimulus-responsive macromolecules and nanoparticles for cancer drug delivery. Nanomedicine (Lond) 5: 793-806, 2010.
19. Fang H, Feng Q, Shi Y, Zhou J, Wang Q and Zhong L: Hepatic insulin resistance induced by mitochondrial oxidative stress can be ameliorated by sphingosine 1-phosphate. Mol Cell Endocrinol 501: 110660, 2020.
20. Do MH, Phan NH, Nguyen TD, Pham TT, Nguyen VK, Vu TT and Nguyen TK: Activated carbon/Fe(3)O(4) nanoparticle composite: Fabrication, methyl orange removal and regeneration by hydrogen peroxide. Chemosphere 85: 1269-1276, 2011.
21. Deng Z, Rong Y, Teng Y, Mu J, Zhuang X, Tseng M, Samykutty A, Zhang L, Yan J, Miller D, *et al*: Broccoli-Derived nanoparticle inhibits mouse colitis by activating dendritic cell AMP-Activated protein kinase. Mol Ther 25: 1641-1654, 2017.
22. Dashamiri S, Ghaedi M, Asfaram A, Zare F and Wang S: Multi-response optimization of ultrasound assisted competitive adsorption of dyes onto Cu (OH)2-nanoparticle loaded activated carbon: Central composite design. Ultrason Sonochem 34: 343-353, 2017.
23. Hou X, Lin H, Zhou X, Cheng Z, Li Y, Liu X, Zhao F, Zhu Y, Zhang P and Chen D: Novel dual ROS-sensitive and CD44 receptor targeting nanomicelles based on oligomeric hyaluronic acid for the efficient therapy of atherosclerosis. Carbohydr Polym 232: 115787, 2020.
24. Li S, Luo L, He Y, Li R, Xiang Y, Xing Z, Li Y, Albashari AA, Liao X, Zhang K, *et al*: Dental pulp stem cell-derived exosomes alleviate cerebral ischaemia-reperfusion injury through suppressing inflammatory response. Cell Prolif 54: e13093, 2021.
25. He F and Zuo L: Redox roles of reactive oxygen species in cardiovascular diseases. Int J Mol Sci 16: 27770-27780, 2015.

26. Kwon JH, Lee NG, Kang AR, Ahn IH, Choi IY, Song JY, Hwang SG, Um HD, Choi JR, Kim J, *et al*: JNC-1043, a novel podophyllotoxin derivative, exerts anticancer drug and radiosensitizer effects in colorectal cancer cells. Molecules 27, 2022.
27. Behera SS, Pramanik K and Nayak MK: Recent advancement in the treatment of cardiovascular diseases: Conventional therapy to nanotechnology. Curr Pharm Des 21: 4479-4497, 2015.
28. Yoshida K, Ono T, Dairaku T, Kashiwagi Y and Sato K: Preparation of hydrogen peroxide sensitive nanofilms by a Layer-by-Layer technique. Nanomaterials (Basel) 8: 941, 2018.
29. Kumari P, Rompicharla SVK, Muddineti OS, Ghosh B and Biswas S: Transferrin-anchored poly(lactide) based micelles to improve anticancer activity of curcumin in hepatic and cervical cancer cell monolayers and 3D spheroids. Int J Biol Macromol 116: 1196-1213, 2018.
30. Kiran Rompicharla SV, Trivedi P, Kumari P, Ghanta P, Ghosh B and Biswas S: Polymeric micelles of suberoylanilide hydroxamic acid to enhance the anticancer potential in vitro and in vivo. Nanomedicine (Lond) 12: 43-58, 2017.
31. Son GM, Kim HY, Ryu JH, Chu CW, Kang DH, Park SB and Jeong YI: Self-assembled polymeric micelles based on hyaluronic acid-g-poly(D,L-lactide-co-glycolide) copolymer for tumor targeting. Int J Mol Sci 15: 16057-16068, 2014.
32. Luo L, He Y, Jin L, Zhang Y, Guastaldi FP, Albashari AA, Hu F, Wang X, Wang L, Xiao J, *et al*: Application of bioactive hydrogels combined with dental pulp stem cells for the repair of large gap peripheral nerve injuries. Bioact Mater 6: 638-654, 2021.
33. Oerlemans C, Bult W, Bos M, Storm G, Nijsen JF and Hennink WE: Polymeric micelles in anticancer therapy: Targeting, imaging and triggered release. Pharm Res 27: 2569-2589, 2010.
34. Nam SH, Lee SW, Lee YJ and Kim YM: Safety and tolerability of weekly Genexol-PM, a Cremophor-Free polymeric micelle formulation of paclitaxel, with carboplatin in gynecologic cancer: A phase I study. Cancer Res Treat 55: 1346-1354, 2023.
35. Liu Y, Liu Y, Zang J, Abdullah AAI, Li Y and Dong H: Design strategies and applications of ROS-Responsive phenylborate Ester-based nanomedicine. ACS Biomater Sci Eng 6: 6510-6527, 2020.
36. Yoshida K, Awaji K, Shimizu S, Iwasaki M, Oide Y, Ito M, Dairaku T, Ono T, Kashiwagi Y and Sato K: Preparation of microparticles capable of glucose-induced insulin release under physiological conditions. Polymers (Basel) 10: 1164, 2018.
37. Council NR, Earth Do, Studies L, Research IfLA, Care CftUotGft and Animals UoL: Guide for the care and use of laboratory animals, 2010.
38. Ovsianikov A, Deiwick A, Van Vlierberghe S, Dubruel P, Moller L, Drager G and Chichkov B: Laser fabrication of three-dimensional CAD scaffolds from photosensitive gelatin for applications in tissue engineering. Biomacromolecules 12: 851-858, 2011.
39. Oommen OP, Duehrkop C, Nilsson B, Hilborn J and Varghese OP: Multifunctional hyaluronic acid and chondroitin sulfate nanoparticles: Impact of glycosaminoglycan presentation on receptor mediated cellular uptake and immune activation. ACS Appl Mater Interfaces 8: 20614-20624, 2016.
40. Neves AR, Queiroz JF, Costa Lima SA, Figueiredo F, Fernandes R and Reis S: Cellular uptake and transcytosis of lipid-based nanoparticles across the intestinal barrier: Relevance for oral drug delivery. J Colloid Interface Sci 463: 258-265, 2016.
41. Zamani E, Johnson TJ, Chatterjee S, Immethun C, Sarella A, Saha R and Dishari SK: Cationic π-Conjugated polyelectrolyte shows antimicrobial activity by causing lipid loss and lowering elastic modulus of bacteria. ACS Appl Mater Interfaces 12: 49346-49361, 2020.
42. Livak KJ and Schmittgen TD: Analysis of relative gene expression data using real-time quantitative PCR and the 2(-Delta Delta C(T)) method. Methods 25: 402-408, 2001.
43. Van Poucke C, Verdegem E, Mangelinckx S and Stevens CV: Synthesis and unambiguous NMR characterization of linear and branched N-alkyl chitosan derivatives. Carbohydr Polym 337: 122131, 2024.
44. Burns J, Wilding CP, L Jones R and H Huang P: Proteomic research in sarcomas-current status and future opportunities. Semin Cancer Biol 61: 56-70, 2020.
45. Musat V, Anghel EM, Zaharia A, Atkinson I, Mocioiu OC, Busila M and Alexandru P: A Chitosan-Agarose Polysaccharide-Based hydrogel for biomimetic remineralization of dental enamel. Biomolecules 11: 1137, 2021.
46. Yuan Z, Nie H, Wang S, Lee CH, Li A, Fu SY, Zhou H, Chen L and Mao JJ: Biomaterial selection for tooth regeneration. Tissue Eng Part B Rev 17: 373-388, 2011.
47. Feng P, Wu P, Gao C, Yang Y, Guo W, Yang W and Shuai C: A multimaterial scaffold with tunable properties: Toward bone tissue repair. Adv Sci (Weinh) 5: 1700817, 2018.
48. Li CJ, Liu XZ, Zhang L, Chen LB, Shi X, Wu SJ and Zhao JN: Advances in bone-targeted drug delivery systems for neoadjuvant chemotherapy for osteosarcoma. Orthop Surg 8: 105-110, 2016.
49. Mauro N, Utzeri MA, Cillari R, Scialabba C, Giammona G and Cavallaro G: Cholesterol-Inulin conjugates for efficient SN38 nuclear delivery: Nanomedicines for precision cancer therapy. Cancers (Basel) 14: 4857, 2022.
50. Song H, Li H, Shen X, Liu K, Feng H, Cui J, Wei W, Sun X, Fan Q, Bao W, *et al*: A pH-responsive cetuximab-conjugated DMAKO-20 nano-delivery system for overcoming K-ras mutations and drug resistance in colorectal carcinoma. Acta Biomater 177: 456-471, 2024.
51. Wang X, Wu J, Lv R, Bai Y, Wang C, Zhang F and Liu Z: Bioinspired hydrogen peroxide-activated nanochannels and their applications in cancer cell analysis. Anal Chem 94: 6234-6241, 2022.
52. Ma L, Zou X and Chen W: A new X-ray activated nanoparticle photosensitizer for cancer treatment. J Biomed Nanotechnol 10: 1501-1508, 2014.
53. Marosfoi MG, Korin N, Gounis MJ, Uzun O, Vedantham S, Langan ET, Papa AL, Brooks OW, Johnson C, Puri AS, *et al*: Shear-Activated nanoparticle aggregates combined with temporary endovascular bypass to treat large vessel occlusion. Stroke 46: 3507-3513, 2015.
54. Meng Y, Chen S, Wang C and Ni X: Advances in composite biofilm biomimetic nanodrug delivery systems for cancer treatment. Technol Cancer Res Treat 23: 15330338241250244, 2024.